 doi:10.20944/preprints202106.0245.v1

Article

A Comprehensive biological and physico-chemical characterization of humic and fulvic acids nanoparticles as a perspective drug

Elena V. Uspenskaya [1,] *, Tatiana V. Pleteneva [1], Tatiana V. Grebennikova [2], Ilaha V. Kazimova [1], Irina T. Fedyakina[2], Varvara V. Lebedeva[2], Oleg E. Latyshev [2], Olesia V. Eliseeva [2], Viktor F. Larichev [2], Timur M. Garaev [2], Tatiana V. Maximova [1], Mariya A. Morozova [1], Pham My Hang [1,] and Anton V. Syroeshkin[1]

[1] RUDN University, Department of Pharmaceutical and Toxicological Chemistry, Medical Institute, 117198, 6 Miklukho-Maklaya Street, Moscow, Russia; uspenskaya75@mail.ru

[2] Federal Government Budgetary Institution "National Research Center for Epidemiology and Microbiology named after Honorary Academician N.F. Gamaleya" of the Ministry of Health of the Russian Federation; t_grebennikova@mail.ru

* Correspondence: uspenskaya75@mail.ru; Tel.: (+7-916-655-79-86)

Abstract: This work presents the results of a comprehensive physico-chemical and biological study of humic substances samples – an extract of humic and fulvic acids. The performed loss on drying test showed a 22 times different dry matter content between EHS and FA. The morphology and distribution of particles in the dry residue of the samples assessed using the methods of optical and digital microscopy demonstrated differences in the qualitative features of the microstructures of their surfaces and granulometries. Shimadzu X-ray fluorescence spectrometry revealed Si (8.1 and 1.7%), P (33.5 and 2.7%), S (4.3 and 59.5%), K (1.35 and 2.5%), Ca (10.9 and 3.2%), Mn (0.27 and 0.06%), Fe (11 and 0.05%), Cu (0.16 and 0.45%), Zn (0.06 and 0.02%) in the dry residues of the EHS and FA samples, respectively. A high intensity of the X-ray fluorescence signal for Fe atoms in the EHS sample was demonstrated. The FT-IR spectra for EHS and FA are characterized by similar vibration frequencies that are characteristic of the chromone derivatives (1-benzopyran-4-one). The UV absorption spectrum is characterized by λ_{max} = 281 nm for FA. The EHS solution showed a fluorescence maximum at λ_{em} = 560 nm at λ_{ex} = 280 nm. Using the DLS method, nanoparticles of 1 nm and 200 nm were detected in EHS and FA diluted solutions, which are likely to condition the biochemical and physical properties of humic acids. Using the Spirotox-test method, the absence of the toxic effect of humic acids on the cell model of ciliates *Sp. ambigua* was established. When the cell model was incubated in a solution of a toxicant of the fluoroquinolone group, a decrease in toxicity was demonstrated when diluted with the EHS solution. The results of the study of the antiviral activity of EHS and FA showed that the study objects in the culture of Vero-E6 cells, in doses nontoxic to cells, suppress the reproduction of the SARS-CoV-2 virus both in the study of the virucidal effect and in the study of the antiviral activity according to the therapeutic and prophylactic model scheme of injection. The results obtained suggest that standardized drugs based on humic acids may open up new perspectives in their biomedical application as antiviral drugs.

Keywords: extract of humic substances; fulvic acid; standardization; nanoparticles of polyelectrolytes; antiviral activity; SARS-CoV-2; VERO-E6; Spirotox-method.

1. Introduction

Humic substances (HS) are complex, heterogeneous, polydisperse mixtures formed in soils, sediments and natural waters as a result of biochemical reactions during the decomposition and transformation of plant and microbial residues (humification) [1]. The first mention of the important role of humic substances in the functioning of plants and

Preprints (www.preprints.org) | NOT PEER-REVIEWED | Posted: 9 June 2021 doi:10.20944/preprints202106.0245.v1

animals is found in the works dated 1761 on agronomic chemistry by the Swedish professor of medicine Johan Gottschalk Wallerius. However, all subsequent decades up to the middle of the 20th century were accompanied by the accumulation of empirical knowledge about the biological role of humic substances in natural soil-forming processes. It was shown that HS are characterized by specificity of composition, structure, properties, depending on the conditions and place of their formation [2-6]. Important components of the humification process are plant lignin, its conversion products, polysaccharides, melanin, cutin, proteins, nucleic acids, and lipids [7]. According to [8], the structure of humic substances as polyfunctional compounds does not have a constant chemical composition, which is explained by the stochastic nature of humification processes [9]. Humic substances are extracted from the soil in the form of alkaline solutions, then subjected to fractionation into humic (HA) and fulvic acids (FA), depending on their different solubility in water [10]. Humic and fulvic acids (*fulvus* — red-yellow) are the most reactive components of humic substances, hypothetical structural models of which are described in [11-13]. Molecules of humic substances of different molecular weights can bind and form a supramolecular humic ~~network~~ structure; the degree of aggregation depends on the pH, ionic strength, and mineral composition of the solution [14]. They are therefore classified as polyelectrolytes (Figure 1).

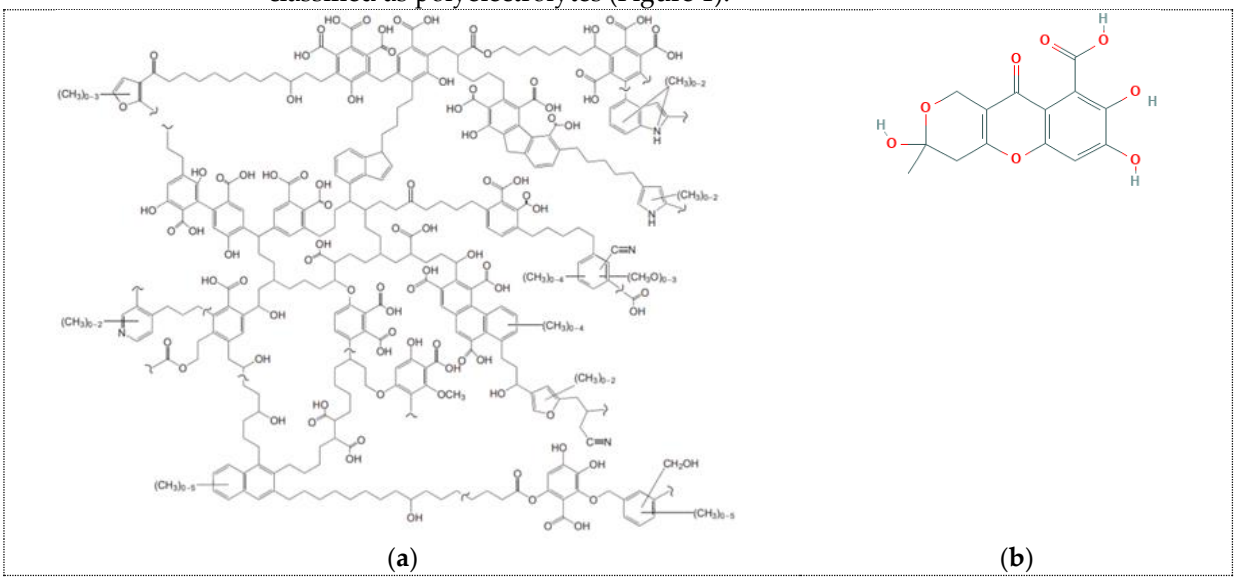

(**a**) (**b**)

Figure 1. Hypothetical molecular structure: (**a**) of Humic acid molecules; (**b**) Fulvic acid; IUPAC Name (3,7,8-trihydroxy-3-methyl-10-oxo-1,4-dihydropyrano[4,3-b] chromene-9-carboxylic acid); M.m.= 308.24 g/mol [15].

As can be seen in Figure 1, humic substances belong to anionic polyelectrolytes, since they contain polar functional groups in their structure – carboxyl, hydroxyl (alcohol, phenolic) ones, able to dissociate with the formation of negatively charged particles. The described property determines the ability of HS to form complexes with heavy metal ions like the Lewis acid-base reaction [16]. The ability of HS to occlude metals determines the content of micronutrients in their solutions in bioavailable forms, as well as the plant metabolism. According to [17], HS are able to immobilize heavy metals and increase their migration ability. The authors of [18] demonstrated ~~a~~ high efficiency of extraction of precious metals (gold and platinum group elements, PGE) from alkaline extracts of HS brown coal, in which highly dispersed particles of elemental gold were stabilized by humic and fulvic acids.

In recent decades, there ~~have~~ appeared numerous publications about studies of the pharmacological activity of HS and FA against human immunodeficiency virus HIV-1 [19], influenza virus [20], herpes simplex virus-1 (HSV-1) [21], tick-borne encephalitis vi-

Preprints (www.preprints.org) | NOT PEER-REVIEWED | Posted: 9 June 2021 doi:10.20944/preprints202106.0245.v1

rus (TBEV) [22], bacteria *Enterococcus faecalis and Klebsiella pneumoniae* [23], and phytopathogenic fungi [24]. The authors demonstrated ~~a~~ much higher activity of the humic acids versus fulvic acids: HA > HMA > FA, as well as the dependence on the source of the humic acid release: coal > peloid > peat. The significant role of active components – aliphatic fragments (for HA) and COOH, OH fragments (for FA), which determine a positive correlation with the inhibition rates of HAs and FAs against phytopathogenic fungi, is discussed. The both sequences follow the trend in lipophilicity index (a ratio of aromatic to aliphatic carbon) for these humic materials [25]. Review publications describe the possible mechanisms of HS and FA effect in preventing the replication of the SARS CoV-2 virus by sorption on the virus envelope protein and thereby blocking the sorption of viral particles on the cell surface [26]. Here are currently no drugs that have shown clear and consistent benefits in treating SARS CoV-2, but numerous trials in different countries are underway suggesting that HS may reduce symptoms.

All these data create prerequisites for the creation of new biologically active substances based on natural polyelectrolytes for the pharmaceutical industry. However, the official use of humic preparations in medicine is limited by the lack of registered drugs based on them, due to the complexity of their standardization. For this reason, solving the problem of HS standardization by methods of physico-chemical and biological study is an urgent task of the modern pharmacy.

The purpose of this work is a comprehensive study of solutions and dry matters of humic, fulvic acids by physico-chemical and biological methods for the development of a promising drug for SARS CoV-2.

2. Results

2.1. Determination of dry residue

Since the determination of dry matter in a liquid sample gives a more convenient idea of the chemical composition of the analyzed material, and also allows comparing different samples with similar physico-chemical properties, we carried out a test to determine the content of the residue after drying samples of humic acid (EHS) and fulvic acid (FA) extracts to a constant mass (Figure 2).

(**a**) (**b**)

Figure 2. Dry residue: (**a**) extract of humic acids; (**b**) fulvic acid.

The tests carried out in accordance with [27] resulted in the determination of the dry residue – $7.34 \cdot 10^{-2}$ g/ml and $3.36 \cdot 10^{-3}$ g/ml, as well as weight loss due to water and volatile substances, which was 92.63% and 99.66%, respectively, for EHS and FA. Thus, the EHS and FA samples differ from each other in terms of the content of soluble compounds and dry residue.

2.2. Optical microscopy

Since the shape, color and size of crystals of a solid are its individual characteristics [28], we studied the morphology and particle distribution of dry samples, invisible to the naked eye, using optical and portable digital microscopy (Figure 3).

Preprints (www.preprints.org) | NOT PEER-REVIEWED | Posted: 9 June 2021 doi:10.20944/preprints202106.0245.v1

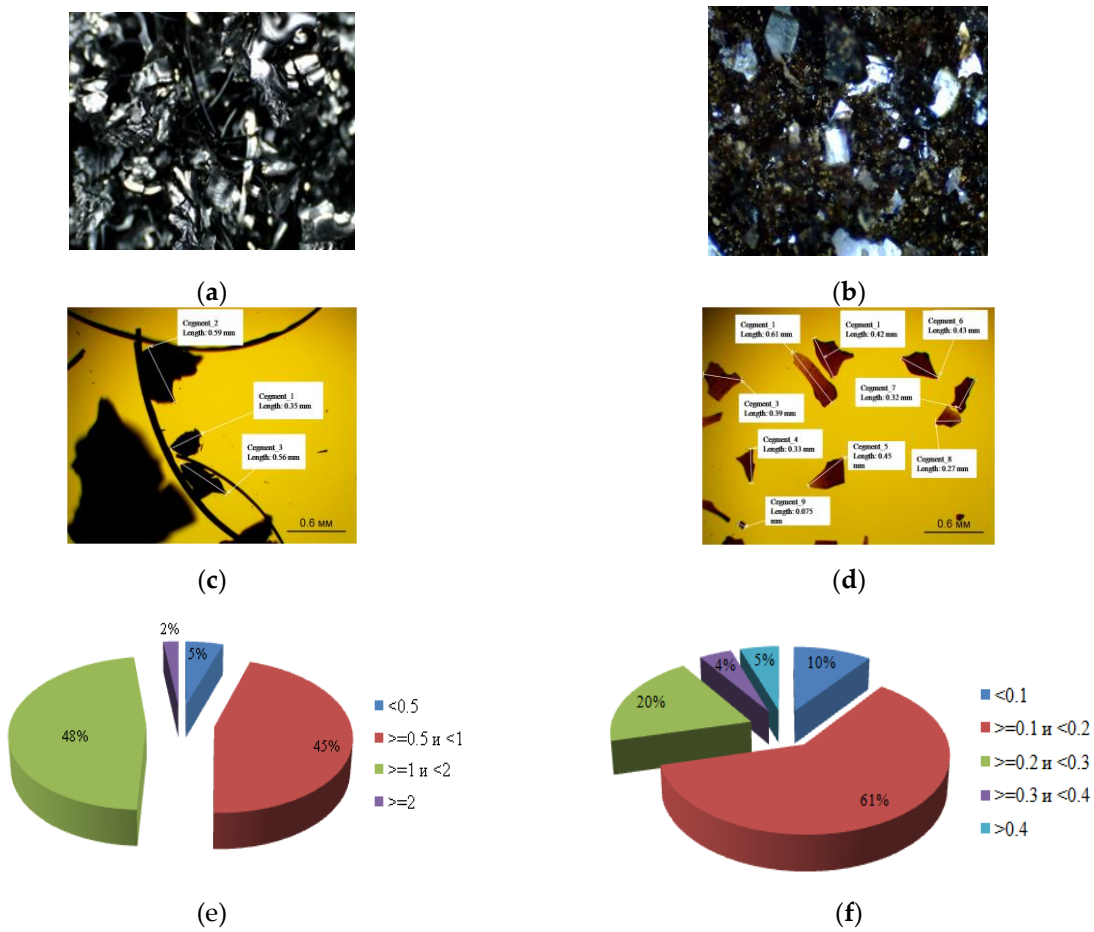

Figure 3. Morphology and particle size distribution in dry samples: (**a), (c), (e)** extract of humic acids; (**b**), (**d**), **(f)** fulvic acid.

It can be seen that the EHS sample contains several mineral phases with different particle shapes (crystals, fragmental particles, complex agglomerates, extended linear structures), a large proportion of which, 48% and 45%, are particles from 0.5 to 2 mm). The FA dry residue sample is a highly dispersed, homogeneous micro-aggregate composition, a large proportion (61%) of which does not exceed 0.1 mm. When viewed through a binocular lens, FA particles are homogeneous, rounded fragments of minerals.

The analysis and digital visualization [29] of the surface relief of the EHS and FA samples demonstrate differences in the qualitative features of their surface microstructure: elongated bodies, accumulation of discrete mineral fragments in the EHS.

2.3. Spectroscopy

2.3.1. X-ray fluorescence spectrometry – elemental analysis

Using energy dispersive X-ray fluorescence (EDXRF), the elemental composition of the test samples in the residue after drying was evaluated (Figure 4).

Preprints (www.preprints.org) | NOT PEER-REVIEWED | Posted: 9 June 2021 doi:10.20944/preprints202106.0245.v1

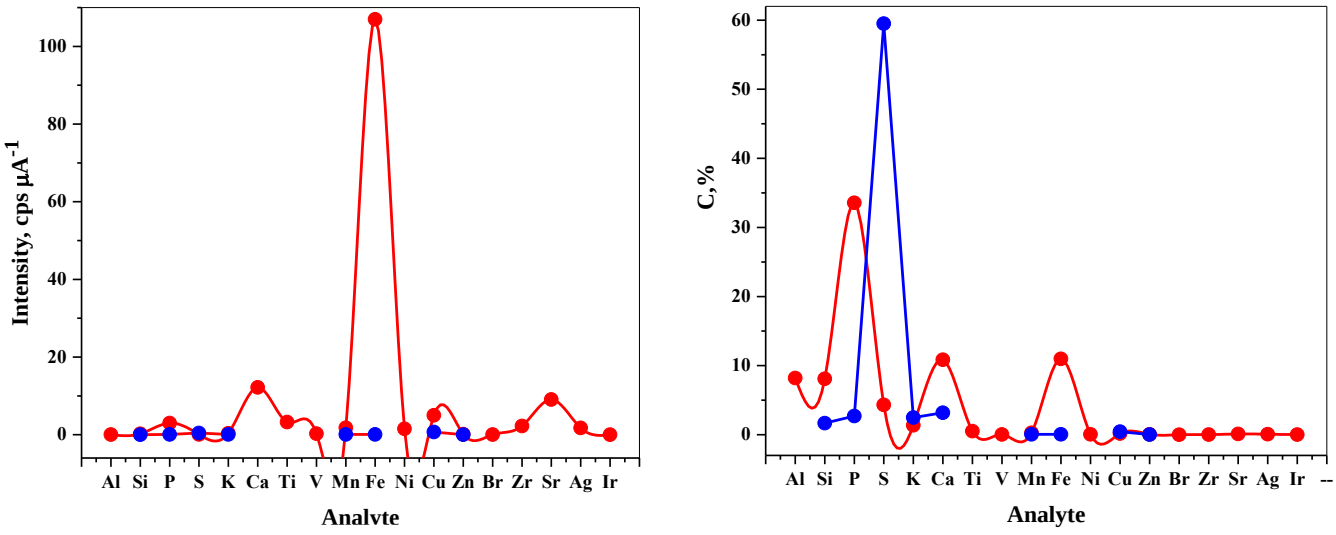

(**a**) (**b**)

Figure 4. X-Ray fluorescence analisys of the elements in dry residue of EHS (red) and FA (blue) samples: (a) intensity dependence ; (b) dependence on element fraction.

As can be seen in Figure 4, atoms of the elements Si, P, S, K, Ca, Mn, Fe, Cu, Zn were found in both EHS and FA samples. Noteworthy is the high intensity of the X-ray fluorescence signal for Fe atoms in the EHS sample. It is known that humic substances, participating in the formation of chelates with iron, contribute to plant nutrition [30]. Depending on the solubility and molecular size of HS, humified fractions of organic matter in soil sediments contribute to the creation of a Fe reservoir available to plants [31]. It has been shown [32-33] that the distribution and release of Fe within plants can be controlled if they are supplied with water-soluble Fe-HS complexes in comparison with other natural or synthetic chelates. In case of Fe, highly stable HS complexes mainly include O-containing groups (carboxyl and phenolic) [34]. Fulvic acids are less prone to the formation of insoluble complexes with metals.

2.3.2. Fourier Transform Infrared (FT-IR) Spectroscopy

The vibrational-rotational spectra of the EHS and FA samples obtained by the disk technique with potassium bromide are shown in Figure 5.

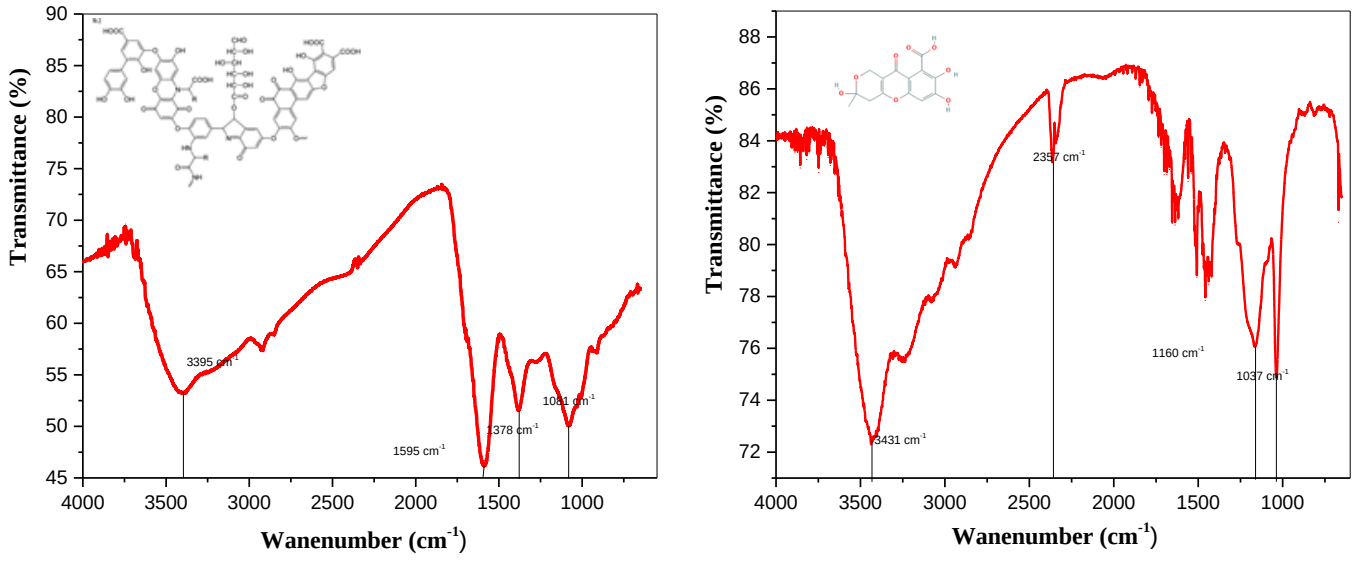

(**a**) (**b**)

Preprints (www.preprints.org) | NOT PEER-REVIEWED | Posted: 9 June 2021 doi:10.20944/preprints202106.0245.v1

Figure 5. FT-IR (Fourier Transform Infrared Spectroscopy) spectrum of: (**a**) Extract of humic substances; (**b**) Fulvic acid sample.

The analysis of the IR spectra of the samples under investigation showed the presence of characteristic light transmission bands corresponding to vibrations of bonds between atoms in the structural fragments of alcohol and phenolic hydroxyls, cyclic ethers, carbonyls, and numerous methylene groups [35].

The EHS spectrum is represented by several characteristic bands at 3395, 1595, 1378, and 1081 cm^{-1}. In a comparative analysis of the transmission spectra of the compounds under investigation, it was found that the EHS sample is characterized by higher values of the extinction coefficients, as a result of which the percentage of light transmission is noticeably reduced, which is probably caused by the nonstoichiometric composition and irregular heterogeneous structure with numerous functional groups. Stretching vibrations of free and bound hydroxyl groups (OH) usually form a broadband region in the frequency range from 3200–3670 cm^{-1} [36]. However, due to the coordinating influence of iron atoms present in the EHS composition and the formation of complex nanostructures containing Me-O bonds, the vibrations of the O-H bond can be shifted to the low-frequency region (≈3400 cm^{-1}). In addition, the stretching vibrations of primary or associated amino groups and, probably, imines, can also be attributed to the absorption band at ≈3400 cm^{-1}. The presence of a carbon skeleton manifests itself as a band of stretching vibrations of the C – H bond at 2900 and 2850 cm^{-1} [37] (Table 1).

Table 1. The main transmittance bands in the IR spectrum of EHS and FA.

Frequency Range, cm^{-1}	Group	Compound Class	Appearance/ Comments
Extract humic substances (HS)			
3550-3200	O-H stretching	alcohol	strong, broad/
2920-2850	C-H stretching	alkane	medium/ bands due to Fe nano-spheres [37]
1650-1580	N-H bending	amine	medium
1690-1640	C=O stretching	conjugated ketone	strong
1390-1310	O-H bending	phenol	medium
1085-1050	C-O stretching	primary alcohol	strong
Fulvic acid (FA)			
3550-3200	O-H stretching	alcohol	strong, broad intermolecular bonded
3100-3000	C-H stretching	alkene	medium
2920–2850	C-H stretching	alkane	medium/ ~~полосы, вызванные наносферами~~ bands due to Fe nanospheres
2275-2250	N-C=O stretching	amide	strong, broad
1650-1566	C=C stretching	cyclic alkene	medium
1440-1395	O-H bending	carboxylic acid	medium
1450	C-H bending	alkane	methyl group
1275-1200	C-O stretching	alkyl aryl ether	strong
1085-1050	C-O stretching	primary alcohol	strong

Preprints (www.preprints.org) | NOT PEER-REVIEWED | Posted: 9 June 2021 doi:10.20944/preprints202106.0245.v1

The obtained vibrational-rotational spectra are determined by the structure of the molecules of humus acids, they are characterized by similar vibration frequencies, the shape of the passbands characteristic of the derivatives of benzo-γ-pyrone (chromone (1-benzopyran-4-one). Thus, the infrared spectroscopy method allowed to confirm structural features of investigated compounds [38-39].

2.3.3 Fluorescence (FL) and ultraviolet (UV)-Spectroscopy

It is well known that compounds, which are concentrated benzene nuclei with oxidized pyran (coumarins, chromones), are fluorophores or chromophores due to their high photostability, large Stokes shift, and intense fluorescence with a high quantum yield [40–42]. The electronic absorption and fluorescence emission spectra of aqueous dilution of the FA and EHS liquid samples are shown in Figure 6. The fluorescence spectra, which are a tool for investigating the effect of the fulvate chromone structure on its optical properties, were recorded at their own excitation wavelength.

As follows from Figure 6 (a), the maximum absorption of fulvate is 281±2 nm, which is associated with the presence of a chromone heterocyclic nucleus in the structure. As a small organic fluorophore containing several condensed nuclei in a fluorescent open form (see Figure 1 (b), the fulvate molecule produces intense violet (360 nm) and low-intensity green (560 nm) fluorescence at an excitation wavelength of 280 nm. The emission peaks in the short- and long-wavelength regions of the FL spectrum can be caused by excited state intramolecular proton transfer (ESIPT), which is characteristic of fragments with intramolecular hydrogen bonds [43].

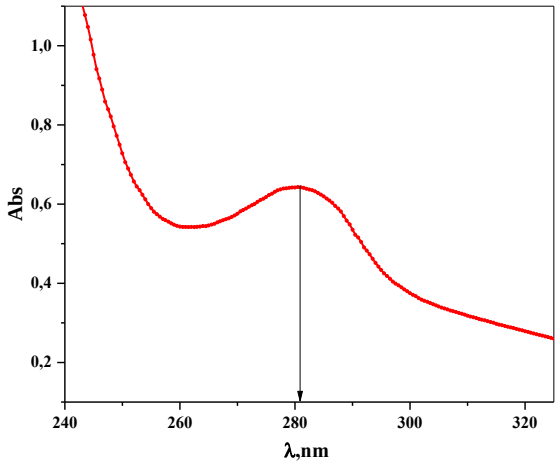

(a)

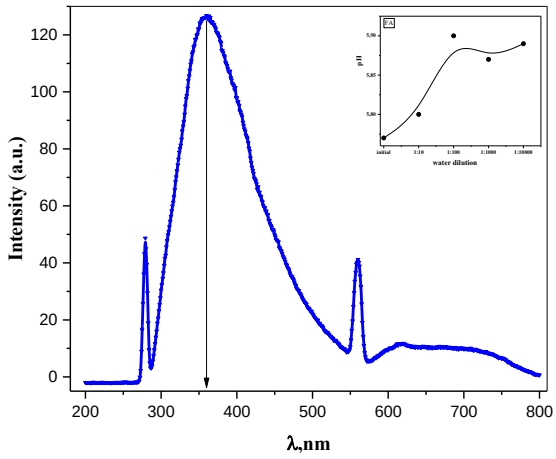

(b)

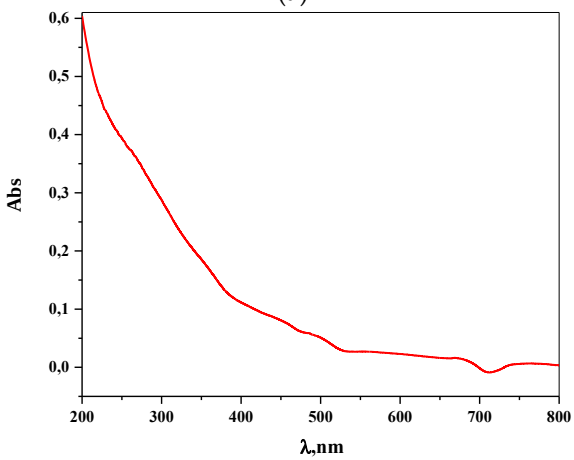

(c)

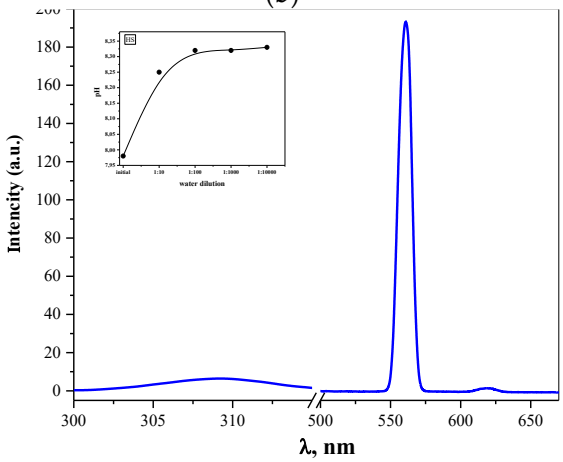

(d)

Preprints (www.preprints.org) | NOT PEER-REVIEWED | Posted: 9 June 2021 doi:10.20944/preprints202106.0245.v1

Figure 6. Fluorescence and ultraviolet spectrum at the excitation wavelength of 280 nm and UV: (a), (b) fulvic acid sample water solution (1:100); (c), (d) extract humic substances sample water solution ($1:10^{12}$). pH Dependence of dilutions are shown in the inserts.

Since the EHS solution demonstrated near-ultraviolet transparency and increased far-ultraviolet absorption in the absence of detectable analytical wavelengths (Figure 6 (c)), it is convenient to characterize the EHS structure by fluorescence spectra (Figure 6 (d)). The photophysical properties of humic acids containing numerous closed cycles, variations of substitutes, and delocalized π-bonds have undergone some changes – the intensity of green fluorescence in the 560 nm region significantly increased.

2.4. Static and Dynamic Light Scattering (SLS/DLS)

The measurement of light scattering of the polyelectrolyte samples allows the estimation of molecular and supramolecular parameters that are important for their identification and characterization. The joint use of the DLS and SLS techniques makes it more efficient to determine particle sizes, aggregation phenomena, interparticle interactions, investigation of the structure and relaxation dynamics of complex fluids when the molecular association/dissociation occurs simultaneously [44-45] (Figure 7).

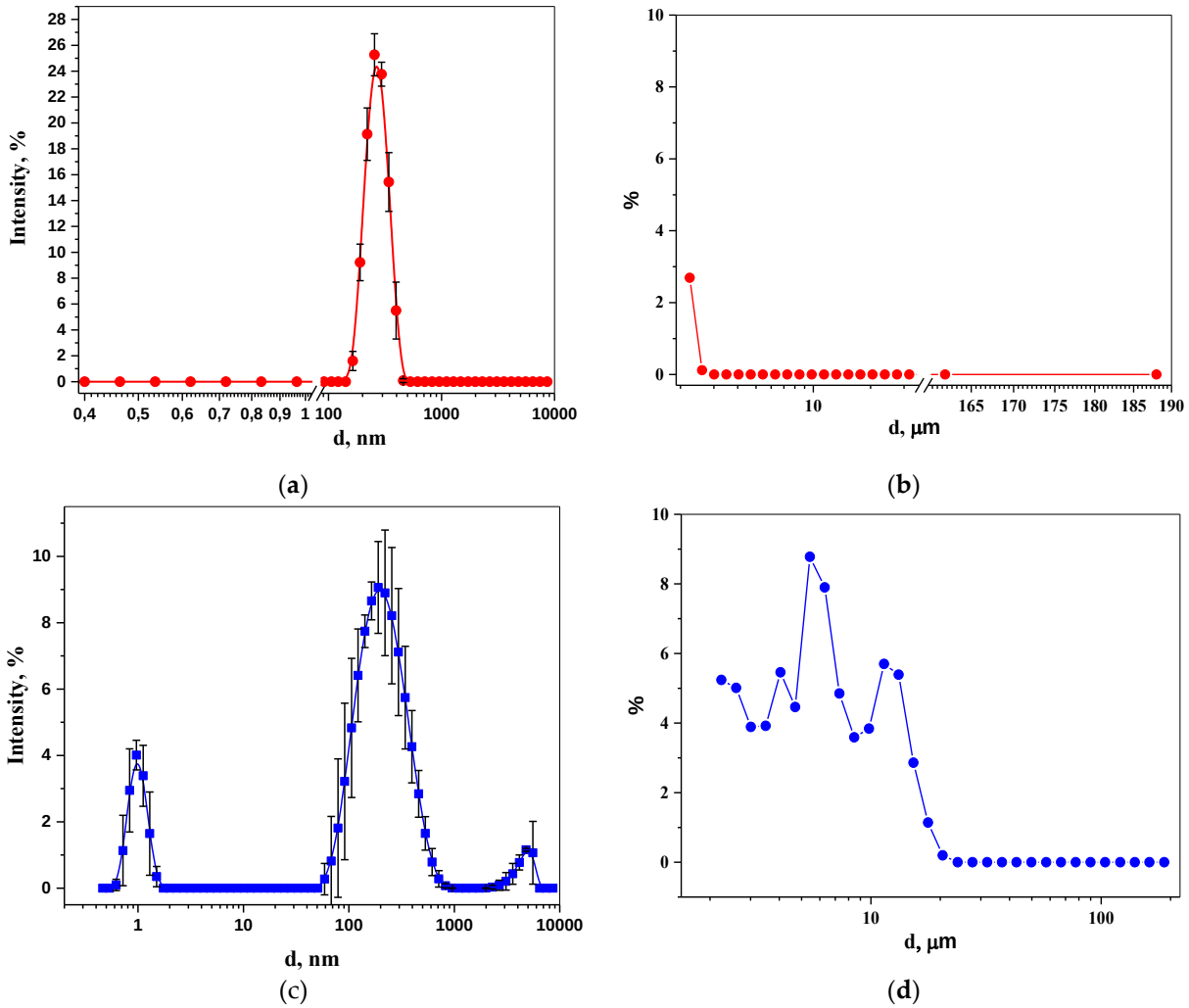

Figure 7. Particle size distribution based on dynamic and static light scattering data: (**a**), **(b)** EHS; **(c)**, **(d)** FA.

The DLS technique in a dilution solution EHS $1:10^4$ detected particles in the monomeric state, occupying the region from 130 nm to 400 nm with a maximum at 200 nm. According to the SLS technique, there are no particles in the size region from 1

Preprints (www.preprints.org) | NOT PEER-REVIEWED | Posted: 9 June 2021 doi:10.20944/preprints202106.0245.v1

to 200 μm. An aqueous dilution (1:2) sample of FA shows a bimodal distribution with peaks at 1 nm and 180 nm according to DLS data. The volume fraction of micron aggregates in the FA sample is distributed over three size groups: 4 μm, 9 μm, 12 μm. Thus, the EHS and FA nanoparticles found in the investigated samples determine their biochemical and physical properties, which predetermine the transfer through cell membranes by different paths solely because of their size. This quality can be used for the delivery of drugs and nucleic acids into cells [46-48].

Further experimental analysis showed the existence of a relationship between the particle size, their biological activity and the efficiency of internalization of nanoparticles by EHS and FA cells.

2.5. Biological activity study

2.5.1. Spirotox-test

The investigation of individual and combined biological activity in accordance with the Arrhenius model of temperature kinetics were carried out using the test culture *Spirostomum ambigua* [49]. The description of the mechanisms of ligand-receptor interaction in the study of the biological activity of substances makes it possible to quantitatively evaluate the biological response of a cellular biosensor to the effect of a toxicant [50].

The existence of a transition state in the process of ligand-induced death of the test object means that the process of cell death occurs with energy consumption. However, the Spirotox experiment using EHS and FA samples demonstrated the absence of toxicity and a significant lifespan of the cellular biosensor in these media. We assume that the reason for the observed phenomenon lies in the unique ability of humified substances to perceive the effects produced without changing properties for an indefinitely long period, showing the effect of the assimilation potential (AP) [51]. To assess the biological activity of EHS, which showed the AP effect, we selected an object of a drug substance with antibacterial action – moxifloxacin hydrochloride (Mxf HCl) – belonging to the fluoroquinolone group. It was found that ligand-induced cell transitions are linearized in Arrhenius coordinates:

$$ln\,k = ln\,A - \frac{E_a}{R} \cdot \frac{1}{T}\,, \qquad (1)$$

where k is the rate constant, Ea is the activation energy, R is the gas constant, A is the pre-exponential factor, and T is the temperature.

In semilogarithmic coordinates, the tangent of the straight-line slope $\ln(1/t_L) = F(1/T)$ to the abscissa axis is E_a/R. The values of observed activation energy (^{obs}Ea) for the test compounds have been found, using Arrhenius coordinates (Table 2).

Table 2. The calculated ^{obs}Ea values of ligand-induced *S. ambigua* death process in water and EHS solutions of Mxf HCl; n=5.

Sample solution	$^{obs}Ea \pm SD$, kJ mol^{-1}
Water solution with 0,094% Mxf HCl	157±2,5
EHS solution with 0,160 % Mxf HCl	196±7

The largest value of activation energy, as well as the increase of *Sp. ambigua* lifetime by about 1,25 times at the same temperature for EHS solution of Mxf HCl compared to water solution of Mxf HCl, indicates higher biological activity of this object.

2.5.2. Determination of the cytotoxic effect of the study objects on the cell culture Vero – E6

The cytotoxic effect was determined by incubation of the investigated humic acids of various concentrations with Vero-E6 cells for 96 h using the MTS vital dye and visual assessment of the cell monolayer. Based on the data obtained in the investigation of the

Preprints (www.preprints.org) | NOT PEER-REVIEWED | Posted: 9 June 2021 doi:10.20944/preprints202106.0245.v1

cytotoxic effect on the culture of Vero-E6 cells using the MTS vital dye, there were constructed analytical curves, from which the CC_{50} was determined for EHS and FA. The concentration that reduced the optical density value by 50% compared to the control cells was 3.19 μg/ml (EHS series 1), 3.13 μg/ml (EHS series 2) and 3.22 μg/ml (EHS series 3). The FA concentration, which reduced the optical density by 50% compared to the control cells, could not be determined, since it was higher than the 1:2 dilution (Figure 8).

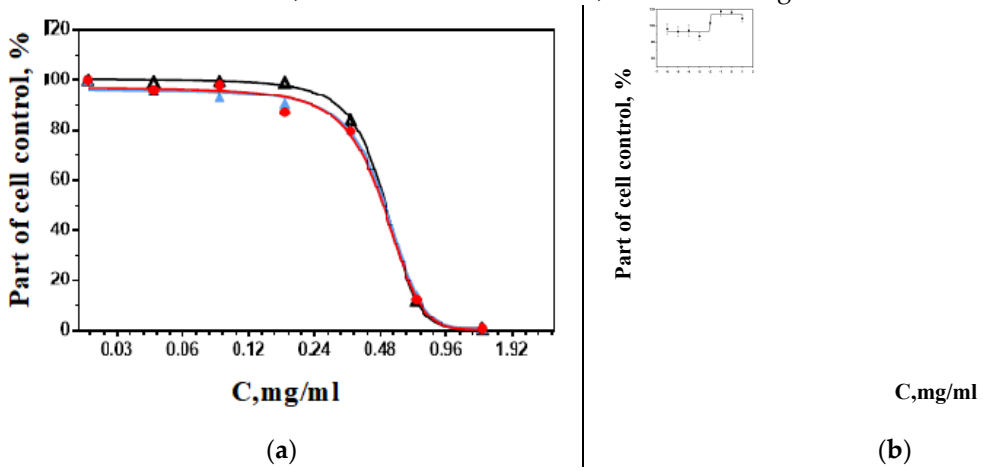

Figure 8. Determination of the cytotoxic effect 96 h after the EHA and FA addition to the transplanted kidney cell line of the African green monkey Vero-E6 (using the MTS vital dye): (a) Humic acid extract, EHS 1 black – CC_{50}=3,19 mg/ml, EHS 2 red – CC_{50}=3,13 mg/ml, EH S 3 blue – CC_{50}=3,22 mg/m.; (b) Fulvic acid CC_{50}=2,0 mg/ml.

Table 3 shows the results of the investigations carried out to study the virucidal and therapeutic-prophylactic activity of three series of the extract of humic acids in concentrations non-toxic for the culture of Vero E6 cells.

Table 3. The effect of EHS on the replication of SARS-CoV-2 in the culture of Vero E6 cells.

EHS test sample	C, mg/ml	Δlg_{max} *
	Virucidal administration regimen	
	0,089	2,89
	0,044	1,89
	0,022	1,0
Series 1	**Therapeutic and prophylactic scheme of administration (1 hour before infection)**	
	0,088	2,87
	0,044	3,75
	0,022	2,0
	Virucidal administration regimen	
	0,088	2,13
	0,044	1,0
	0,022	0
Series 2	**Therapeutic and prophylactic scheme of administration (1 hour before infection)**	
	0,088	2,87
	0,044	1,75
	0,022	0,87
Series 3	**Virucidal administration regimen**	

Preprints (www.preprints.org) | NOT PEER-REVIEWED | Posted: 9 June 2021 doi:10.20944/preprints202106.0245.v1

	0,088	3,75
	0,044	1,75
	0,022	0
	Therapeutic and prophylactic scheme of administration (1 hour before infection)	
	0,088	2,87
	0,044	2,75
	0,022	1,75

* Reduction of the virus infectivity infectious titer with the drug compared with the control virus expressed in decimal logarithms

Thus, in the investigation of the virucidal activity at a concentration of 0.022 mg/ml, EHS2 and EHS3 did not have an inhibitory effect on the reproduction of SARS-CoV-2, EHS1 showed a weak inhibitory effect. Moreover, (EHS2) showed the weakest inhibitory effect in the study of the virucidal activity at a concentration of 0.044 mg/ml and in the study of the antiviral activity according to the therapeutic-prophylactic model scheme at a concentration of 0.022 mg/ml, suppressing the reproduction of the SARS-CoV-2 virus by ≤ 1.0 lg.

Based on the primary data obtained for EHS1, EHS2, EHS3, there were constructed analytical curves, from which 50% inhibitory concentration was determined (IC_{50}). The results for virucidal and therapeutic-prophylactic schemes of injecting the extract of humic substances are shown in Figure 9.

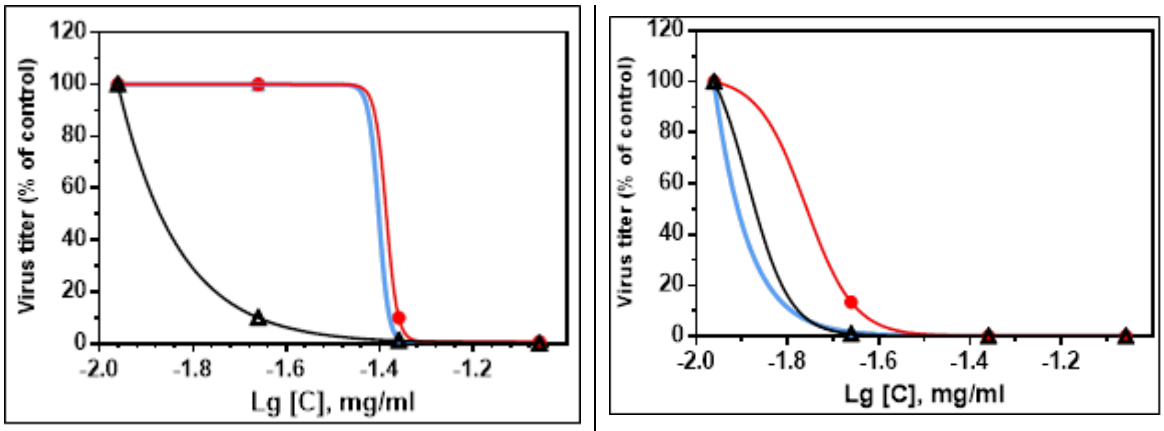

(**a**) (**b**)

Figure 9. Determination of the IC_{50} of humic acid extracts against SARS-CoV-2 in Vero E6 cell culture: **(a)** Humic acid extract with a virucidal scheme, EHS 1 black – IC_{50}=0,002 mg/ml, EHS 2 red – IC_{50}=0,041 mg/ml, EHS 3 blue – IC_{50}=0,039 mg/mL; **(b)** Humic acid extract with a therapeutic and prophylactic scheme, EHS1 black – IC_{50}=0,013 mg/ml, EHS2 red – IC_{50}=0,017 mg/ml, EHS3 blue – IC_{50}=0,007 mg/m.

In the therapeutic-prophylactic model scheme of injection, FA inhibited the replication of SARS-CoV-2 in Vero E6 cell culture at concentrations of 0.2 mg/ml, 0.1 mg/ml, reducing the virus infectivity titer by 1.75-1.0 1g $TCID_{50}$ (tissue culture infectious dose), respectively. Based on the primary data, there was constructed an analytical curve, from which 50% inhibitory concentration (IC_{50}) was determined (Figure 10):

Preprints (www.preprints.org) | NOT PEER-REVIEWED | Posted: 9 June 2021 doi:10.20944/preprints202106.0245.v1

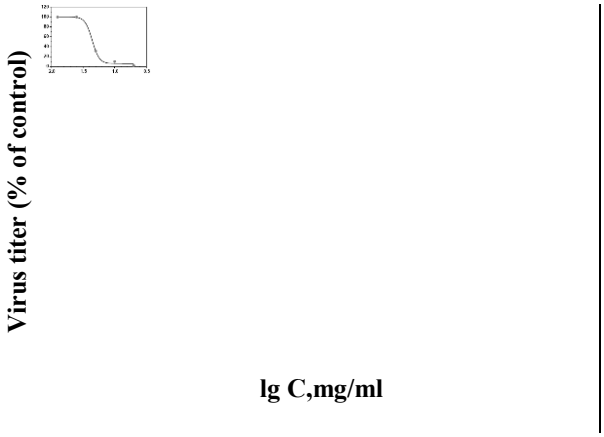

Figure 10. Determination of the IC_{50} of the drug Fulvic against SARS-CoV-2 in Vero E6 cell culture.

Table 5 shows the results of the cytotoxic and antiviral activities of EHS and FA against the SARS-CoV-2 virus in the Vero E6 cell culture.

Table 5. Consolidated data on cytotoxic and antiviral activity EHS and FA.

Test sample	CC_{50}, mg/ml	Antiviral activities against the SARS-CoV-2 virus		
		Δlg_{max}	IC_{50}, mg/ml	SI
Virucidal administration regimen				
EHS 1	3,19	2,89	0,002	1593,5
EHS 2	3,13	2,13	0,041	76,3
EHS 3	3,22	3,75	0,039	82,4
Treatment and prevention model scheme				
EHS 1	3,19	3,75	0,013	245
EHS 2	3,13	2,87	0,017	184
EHS 3	3,22	2,87	0,007	459,3
FA	2	1,75	0,044	45,5

3. Discussion

The humus acids are high molecular weight polyelectrolytes, the structural units of which are represented by aromatic condensed systems with side chains and heterocycles [52]. The physico-chemical properties of the humus acids, including humic, fulvic, and other acids extracted by alkali solutions were investigated with the involvement of a significant fleet of equipment [53]. However, the properties of the humic and fulvic acids can vary depending on the medium of their formation – humification [54]. This is the reason for many publications about the properties of the humus acids. All this leads to an unambiguous decision on the need for standardization and development of quality control methods for the components of the humus acids.

This problem is especially relevant in connection with the data appearing in the literature on the significant biological activity of the components of humus acids – antitumor, antibacterial, antifungal, antiviral [55-57]. Due to the massive spread of new strains of the coronavirus infection, the development of drugs that suppress the replication of the SARS-CoV-2 virus is urgent [58].

The results of this study of the antiviral activity showed that the study objects in the culture of Vero-E6 cells, in doses non-toxic to cells, suppress the reproduction of the SARS-CoV-2 virus both in the study of the virucidal effect and in the study of the antiviral activity according to the therapeutic-prophylactic model scheme of injection. The difference in activity of different EHS series can be related to its heterogeneity and sophisticated complex composition (see Figure 1). According to the criteria for evaluating the antiviral

 doi:10.20944/preprints202106.0245.v1

effect of drugs in vitro, compounds, in which the decrease in the virus titer in concentrations non-toxic for the cell culture is at least 1.5–2.0 lg and SI≥8, exhibit pronounced activity.

The properties and widespread medical application of nanoparticles to enhance contrast in magnetic resonance imaging, in immunoassays and drug delivery are well known from the literature [59]. The internalization of nanoparticles and their absorption by cells, depending on the size, have been shown [60]

The results of our research have shown that the composition of the components of humus acids includes occluded metal nanoparticles in addition to the organic structure of nonstoichiometric composition and an irregular heterogeneous structure with many functional groups. Apparently, their presence determines their properties as nanocontainers [61]. Objects that are not characterized by nanosized particles completely lose the described properties [62]. Our studies emphasize that the consideration of the humus acids and their components – humic and fulvic acids from the standpoint of metal-organic nanosized objects can explain the detected virucidal activity, as well as become a potential object for creating a promising standardized drug.

4. Materials and Methods

4.1. Materials

4.1.1. EHS and FA Samples

A natural complex of humic-fulvic acids isolated from low-lying peat, sapropel and some varieties of brown coal (leonardite) using the technology of the VimaVita Company (Sistema-BioTechnologii LLC, RF). The HS concentrate containing humic acids (HA), himatomelanic acids (HMC), fulvic acids (FA), humus acids (HFA) and structural analogs of humic substances was obtained by the method of oxidative-hydrolytic destruction of lignin-containing raw materials (solid-phase fermentation) with subsequent purification [63]. As a result of high-intensity acoustic cleaning, a concentrated viscous colloidal disperse system of humic substances of dark brown color was obtained for research. (pH=7.98±0.1).

Fulvic acid extract (Terra Aquatica, France) in the form of a liquid, transparent solution of brown color, obtained by extraction from a special type of brown coal leonardite (pH=5,77±0,1).

To study the physico-chemical properties of HS and FA, aqueous solutions of the initial concentrate were prepared. All solutions of humic substances fractions were stored at +4°C.

4.1.2. Cell Culture. The study was carried out on a finite kidney cell line of the African green monkey (Chlorocebus aethiops) Vero-E6. MEM medium with glutamine (Capricorn Scientific GmbH, Germany) containing 10% and 2% fetal calf serum (Biosera, USA) respectively and gentamicin (50 μg / ml) (Capricorn Scientific GmbH, Germany) was used as a growth medium (GM) for growing cells and as a supporting medium (SM) for setting up a reaction. Vero-E6 cells were cultured in 96-well plates in a volume of 100 μl of GM for 24 h at 37°C in an atmosphere with 5% CO_2. The inoculation dose was 18,000 cells/well.

4.1.3. Virus. The study used the SARS-CoV-2 human coronavirus, passage 3, with infectivity of $10^{7.5}$ $TCID_{50}$/ml. Strain description: hCoV-19/Russia/Moscow-PMVL-12/2020 (EPI_ISL_572398) GISAD: PMVL-12. Booking reference EPL_ISL_572398.

4.1.4. Study Design. The study of the antiviral activity of the study objects was carried out in accordance with the requirements of the Pharmacological State Committee of the Russian Federation for the experimental (preclinical) study of new pharmacological substances. The study included: determination and assessment of the cytotoxic effect of the study objects on the morphology and viability of Vero-E6 cells, as well as the study of the antiviral activity against SARS-CoV-2.

4.2. Determination of the cytotoxic effect of the study objects on the cell culture Vero – E6.

Multiple dilutions of the study objects were prepared in plates by titration in 7-8 wells with a step of × 2 on GM medium. The solutions of the study objects were transferred in 200.0 μl into the wells of the test plates with cells. Each point was tested in 4 parallel

Preprints (www.preprints.org) | NOT PEER-REVIEWED | Posted: 9 June 2021 doi:10.20944/preprints202106.0245.v1

rows of plate wells. 200 µl of SM without study objects was used as a control of the state of the cell culture. The plates were incubated for 96 hours at 37±0.5°C in atmosphere with 5% CO_2. The state of the cell monolayer was visually assessed to identify destructive changes and changes in the morphology of the cell monolayer. After 96 hours, the culture medium was removed and 100 µl of GM and 20 µl of vital dye (MTS) (CellTiter 96® AQueous One Solution Cell Proliferation Assay, Promega, G3582) were added to each well. After incubation for 3 hours at 37±0.5°C, the results were recorded on a BIO-RAD reader at a wavelength of 490 nm, the reference wave was 630 nm. The concentration of the test substance, which reduces the optical density value by 50% compared to the control cells, was taken as the 50% cytotoxic dose (CC_{50}).

4.3. In Vitro Study of the Antiviral Activity of EHS and FA.

At the second stage of the study, the virucidal activity against SARS-CoV-2 of three series of the extract of humic substances was studied, as well as their antiviral activity according to a therapeutic-prophylactic model scheme. Each series of the drug was tested at three concentrations. The antiviral activity of the Fulvic drug was studied using a therapeutic-prophylactic model scheme at 4 concentrations. The selection of concentrations for the studies of antiviral activity was carried out on the basis of the results of the study of cytotoxic action within the range of concentrations that are not toxic to cells (i.e., lower than the CC_{50} value).

When studying the virucidal effect, the selected dilutions of the drugs (according to CC_{50}) were mixed with dilutions of the virus (from 10^{-1} to 10^{-7}) in equal volumes of 100 µl and incubated for 1 hour at 37±0.5°C in atmosphere with 5% CO_2 and transferred to a plate with a monolayer of washed cells. To study the antiviral activity according to the therapeutic-prophylactic model scheme, working dilutions of the study objects were added to the cells 1 hour before infection with the virus and incubated at 37±0.5°C in an atmosphere of 5% CO_2.

As a control, we used SARS-CoV-2 virus dilutions from 10^{-1} to 10^{-7} without adding study objects. Each drug concentration was tested in four parallel rows of plate wells. The plates were incubated for 96 hours at 37±0.5°C in atmosphere with 5% CO_2. The antiviral activity was assessed visually under a microscope 96 hours after infection by inhibition of the cytopathic effect (CPE) of the virus on the cells. The result was assessed by Δlg_{max} – the maximum decrease in the value of the infectious viral dose in the experiment in comparison with the control expressed in decimal logarithms.

4.4. Statistical Data Processing

The calculation of the values of 50% cytotoxic concentration (CC_{50}) and 50% effective concentration (IC_{50}) was performed by methods generally accepted for biological research using the Microsoft Excel 5.0 and GraphPad Prism 6.01 software package. The 4-parameter equation of the logistic curve (menu items "Nonlinear regression" – "Sigmoidal dose-response (variable slope)") was adopted as a working model for the CC_{50} analysis. The 4-parameter equation of the logistic curve (menu items "Nonlinear regression" - "log (inhibitor) vs. response (variable slope)") was adopted for the analysis of IC_{50}. Based on the data obtained, SI was calculated using the equation: $SI = CC_{50}/IC_{50}$.

4.5. Loss on drying (LOD)

The determination of the mass loss of extract of humic substances and liquid fulvic acid on drying was carried out according to the requirements [27]. For this purpose, the accurately measured weight of the tested liquid substance, pre-dried and brought to constant weight, was placed in an evaporating dish (porcelain). The drying was carried out in at 105±5°C for 6 hours in a drying oven BINDER FD (Germany) that provides uniform heat treatment of the entire usable chamber volume [65]. The weight of the sample dish was determined and recorded every hour by removing the dish from the oven and allowing it to cool at room temperature in a desiccator for 30 minutes. The loss on drying (%) was calculated according to the Table 6 and following equation:

$$w = \frac{m_2 - m_3}{m_2 - m_1} \cdot 100\%, \quad (1)$$

Preprints (www.preprints.org) | NOT PEER-REVIEWED | Posted: 9 June 2021 doi:10.20944/preprints202106.0245.v1

were m_1 is the weight of the measuring cup brought to a constant weight (g); m_2 is the weight of the measuring cup containing the tested sample before drying (g); m_3 is the weight of the measuring cup containing the tested sample after drying (g).

Table 6. Determination of weight loss on drying the samples of the extract of humic substances and fulvic acid.

Extract humic substances (EHS)				
t, h	**m_1, g**	**m_2, g**	**$m_{(tested\ liquid\ substance)}$ g**	**Loss on drying (LOD), %**
0	118,6004	127,2238	8,6234	
1		119,2702	0,6698	
2		119,2473	0,6469	
3		119,2411	0,6407	
		m_3, g		
4		119,2362	0,6358	
5		119,2362	0,6358	
6		119,2362	0,6358	
				92,63
Fulvic acid (FA)				
t, h	**m_1, g**	**m_2, g**	**$m_{(tested\ liquid\ substance)}$ g**	**Loss on drying (LOD), %**
0	115,3210	120,1194	4,7984	
1		115,3398	0,0188	
2		115,3391	0,0181	
3		115,3387	0,0177	
		m_3, g		
4		115.3371	0,0161	
5		115.3371	0,0161	
6		115.3371	0,0161	
				99,66

The weight loss on drying test carried out in this manner allowed the determination of the EHS and FA content of non-volatile substances in the samples, as well as the weight loss on drying.

4.6. Optical Microscopy (OM)

Determination of the size, shape, and granulometric composition of the dry residue in the EHS and FA samples was carried out using a microscope with a special binocular attachment (Altami BIO 2, Russia) with magnification 10X (linear field of view 20 mm). To do this, a sample of dry matter was distributed on a glass slide without adhesion of particles. The preliminary calibration was carried out using a micrometer object with a scale of 1DIV = 0.01 mm. The particles were observed in separate fields of view. The length was measured on microscopic images and the shape of the particles was determined using the Altami Studio 3.3 software [66].

4.6.1. Digital Microscopy (DM)

The surface structure of powdery substances obtained after drying the EHS and FA samples was investigated using a portable USB digital microscope LX200 (Levenhuk DTX 50, USA) to determine the size of objects from 1 to 50 μm [67]. The microscope is equipped with a built-in digital 1.3 megapixel camera connected to a computer. The advantage of the digital microscope is the express diagnostics of large sample areas without sample

Preprints (www.preprints.org) | NOT PEER-REVIEWED | Posted: 9 June 2021 doi:10.20944/preprints202106.0245.v1

preparation. The analysis of the structure, relief and defects of the layers adjacent to the surface allowed us to identify the objects under study.

4.7 X-ray Fluorescence (XRF)

An energy dispersive X-ray fluorescence spectrometer (EDX-7000P, Shimadzu Europa GmbH) based on a silicon drift detector with thermoelectric cooling equipped with the PCEDX-Navi software package was used to carry out the nondestructive elemental composition of powder and liquid EHS and FA samples. The range of elements measured by the X-ray fluorescence method is from 11Na to 92U; the X-ray generator is a tube with Rh-anode, current 1–1,000 μA; the irradiated area controlled by the collimator was 10 mm [68]. Pelleted powder or liquid sample of EHS and FA was placed in a closed cuvette covered with a mylar (lavsan) film in air atmosphere and placed exactly in the center of the instrument window. The intensity of the secondary fluorescent radiation was measured to determine the elemental composition of the sample. The study time was 50 seconds for each element (group).

4.8. Fourier-Transform IR Spectroscopy

To obtain and analyze the vibrational spectra of the EHS and FA samples in the spectral range from 4,000 to 750 cm $^{-1}$, an IR Fourier spectrophotometer (Agilent Cary 630, USA) with a transmission attachment was used [69]. Sample preparation – solid residue after drying – for spectrum recording was carried out in accordance with the requirements[70]. For this, about 1 mg of dry residue was triturated with 400 mg of carefully ground and dried potassium bromide until uniform state and compressed for 3-5 minutes to obtain a disk diameter of about 13 mm to have a spectrum of a suitable intensity.

4.9. Fluorescence and UV-Spectroscopy

To obtain the fluorescence spectra of a series of dilutions of the EHS and FA samples, we used an AGILENT Cary Eclipse spectrofluorimeter (USA) with two ultrafast scanning monochromators. The excitation wavelength was 280 nm. The fluorescence spectra in the range from 300 to 800 nm with the maxima of violet and green fluorescence was studied. The absorption spectrum of an aqueous dilution blank (1:100) of FA was obtained in the range from 200 nm to 350 nm using AGILENT Cary 60 equipment (USA).

4.10 Determination of Particle Sizes of Dispersed Systems

To determine the particle size of dispersed systems, the methods of static and dynamic light scattering of aqueous dilutions of EHS and FA were used.

4.10.1. Static and Dynamic Light Scattering (SLS/DLS)

The particle size analysis (volumetric distribution on an ensemble of particles by size/size spectra) was recorded by static light scattering (Low-angle laser light scattering, LALLS) using a MasterSizer 3600 Ec small-angle laser dispersion meter (Malvern, UK) [71-72]. The optical module of the equipment used makes it possible to determine the size of the dispersed phase particles in the range from 1 μm to 180 μm based on the measurement of the angular dependence of the intensity of the scattered laser light passing through the dispersed sample [73]. For the granulometric analysis of the samples under investigation, there were used dilutions of EHS and FA in water 1:1000 and 1:2, respectively.

A Zetasizer Nano ZSP (Malvern, UK) based on dynamic light scattering (DLS) was used to measure the size of nanoparticles in the EHS and FA samples from 0.1 nm to 10,000 nm. DLS technology measures particle diffusion due to Brownian motion with its subsequent transformation into size according to the Stokes-Einstein equation [74]:

$$\boldsymbol{D} = \frac{\boldsymbol{k_B T}}{\boldsymbol{6\,\pi\eta r'}} \quad (2)$$

Preprints (www.preprints.org) | NOT PEER-REVIEWED | Posted: 9 June 2021 doi:10.20944/preprints202106.0245.v1

were D is the diffusion coefficient, k_B is the Boltzmann constant, T is an absolute temperature, η is the liquid viscosity, r is the particle radius.
The dispersion analysis was performed using a Malvern ZetaSizer Nano ZS series analyzer.

4.11. Spirotox Method

The study of the biological activity of aqueous dilutions of EHS in the presence of fluoroquinolone supplement was carried out using the cell culture *Spirostomum ambigua* [75-76]. The mechanism of ligand-receptor interaction includes the stage of interaction of the xenobiotic with the cell, the disintegration of the intermediate complex, accompanied by a change in the concentration of the cellular biosensor due to conformational changes in the receptor, degradation, synthesis of new receptors and the formation of the intermediate state C· Ln (Figure 12).

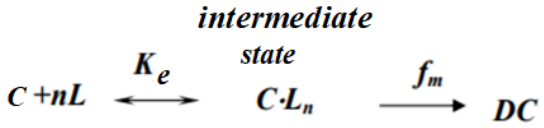

Figure 12. Kinetic scheme of ligand-receptor interaction S. ambigua with toxicant: C-cell, L-ligand, n-stoichiometric coefficient, C. Ln – intermediate state (cell after interaction with the ligand), Ke is the equilibrium constant fast stage, f_m is the rate constant of the cell transition to the dead state, DC is a dead cell [77].

5. Conclusions

A comprehensive study of the properties of humus acids drugs – an extract of humic substances and fulvic acid – was carried out using gravimetric, optical and biological methods. The dry matter content of the samples differs by a factor of 22, the weight loss due to volatiles on drying is 92.63%, 63 and 99.66% for EHS and FA, respectively. The X-ray fluorescence analysis showed a high content of Fe and Cu in the samples. The fluorescence intensity and the number of determined elements increase significantly when the samples are dried. The elemental composition indicates the possible formation of water-soluble Fe/Cu-HS complexes, which are necessary in nature for plant nutrition. This can explain the absence of toxicity of the humus acids when the cell model is exposed to the Spirotox method. Nanoparticles detected by the DLS technique in the range from 1 nm to 200 nm in the HS samples can have a structure of lipid-like objects with occluded iron penetrating through cell membranes into an organic matrix, which was demonstrated by the suppression of the SARS-CoV-2 reproduction in the Vero-E6 cell culture. The IR spectroscopy has demonstrated the appearance of bands characteristic of Fe nanoparticles. The structure of chromone (benzo-γ-pyrone) in samples of humus acids has also been proven, which is a powerful fluorophore and chromophore according to FL and UV spectroscopy methods. Thus, samples of humate chromone can be of important interest and be promising candidates for practical application in the fields of biomedicine after quality and biological activity tests.

Author Contributions: Conceptualization, A.V.S., T.V.G. and T.V.P.; methodology, E.V.U., A.V.S.; investigation, I.V.K., V.V.L., I.T.F., O.V.E.; validation, V.F.L., T.M.G.; data curation, A.V.S., T.V.G. and E.V.U.; formal analysis, I.V.K; writing—original draft preparation, E.V.U.; writing—review and editing, A.V.S., T.V.G. and T.V.P. All the authors discussed the results and commented on the manuscript.

Funding: This research received no external funding.

Institutional Review Board Statement: Not applicable.

Informed Consent Statement: Not applicable.

 doi:10.20944/preprints202106.0245.v1

Acknowledgments: This paper was supported by the RUDN University Strategic Academic Leadership Program

Conflicts of Interest: The authors declare that there are no conflicts of interest regarding the publication of this paper.

Sample Availability: Samples of the compounds are available from the authors.

Abbreviations

COVID-19	Corona Virus Disease 2019
CC_{50}	half maximal cytotoxic concentration
CPA	cytopathic action
DLS	dynamic light scattering
EHS	extract humic substances
$^{obs}E_a$	obseved activation energy
ESIPT	excited state intramolecular proton transfer
EDXRF	energy dispersive X-ray fluorescence
FA	fluvic acids
FRO	ferric chelate reductase
GE	growth environment
HA	humic acids
HS	humic substances
HMA	hymatomelanic acid
IC_{50}	half maximal inhibitory concentration
IHS	insoluble HS
HIV-1	human immunodeficiency virus
HSV-1	simplex virus-1
IRT	iron transporter
IR	infra-red
MEM	minimum essential medium (alpha 1X)
MTS	vital dye (1-solution methyl thiazolyl tetrazolium)
SE	supportive environment
SI	selectivity index
SARS-CoV-2	severe acute respiratory syndrome-related coronavirus 2
SLS	static light scattering
Spirotox test	Spirostomum Ambiguum Acute Toxicity Test
TBEV	tick-borne encephalitis virus
TCID50	50% tissue culture infectious dose
WEHS	water extractable humic substances
Vero-E6	cell culture derived from epithelial buds of African green monkey and transfected with a viral gene

References

1. International Humic Substance Society. Available online: https://humic-substances.org.
2. Wei, X.; Yang, Y.; Shen, Y.; Chen, Z.; Dong, Y.; Wu, F.; Zhan, L. Effects of Litterfall on the Accumulation of Extracted Soil Humic Substances in Subalpine Forests. *Front Plant Sci* **2020**, *5*, 254.
3. Li, Y.; Guo, L.X.; Zhou, Q.Z.; Chen, D.; Liu, J.Z.; Xu, X.M.; Wang, J.H. Characterization of Humic Substances in the Soils of Ophiocordyceps sinensis Habitats in the Sejila Mountain, Tibet: Implication for the Food Source of Thitarodes Larvae. *Molecules* **2019**, *10*, 246.
4. Meng, F.; Yuan, G.; Wei, J.; Bi, D.; Ok, Y.S.; Wang, H. Humic substances as a washing agent for Cd-contaminated soils. *Chemosphere* **2017**, *81*, 461-467.
5. Wnuk, E.; Waśko, A.; Walkiewicz, A.; Bartmiński, P.; Bejger, R.; Mielnik, L.; Bieganowski, A. The effects of humic substances on DNA isolation from soils. *PeerJ* **2020**, *24*, 9378.

6. Shah, Z.H.; Rehman, H.M.; Akhtar, T.; Alsamadany, H.; Hamooh, B.T.; Mujtaba, T.; Daur, I.; Al Zahrani, Y.; Alzahrani, H.A.S.; Ali, S.; Yang, S.H.; Chung, G. Humic Substances: Determining Potential Molecular Regulatory Processes in Plants. *Front Plant Sci* **2018**, *13*, 263.
7. Zech, W.; Senesi, N.; Guggenberger, G.; Kaiser, K.; Lehmann, J.; Miano, T.M.; Miltner, A.; Schroth, G. Factors controlling humification and mineralization of soil organic matter in the tropics. *Geoderma* **1997**, *79*, 117-161.
8. Zhernov, Y.V.; Konstantinov, A.I.; Zherebker, A.; Nikolaev, E.; Orlov, A.; Savinykh, M.I.; Kornilaeva, G.V.; Karamov, E.V.; Perminova, I.V. Antiviral activity of natural humic substances and shilajit materials against HIV-1: Relation to structure. *Environ Res* **2021**, *193*, 110312.
9. Lomovskiy, I.; Bychkov, A.; Lomovsky, O.; Skripkina, T. Mechanochemical and Size Reduction Machines for Biorefining. *Molecules* **2020**, *16*, 5345.
10. Zanin, L.; Tomasi, N.; Cesco, S.; Varanini, Z.; Pinton, R. Humic Substances Contribute to Plant Iron Nutrition Acting as Chelators and Biostimulants. *Front Plant Sci* **2019**,*22*, 675.
11. Stevenson, F. J. Humus chemistry : genesis, composition, reactions.; Publisher: New York, Wiley, 1982; pp. 443.
12. Kleinhempel, D. Ein Beitrag zur Theorie des Huminstoffzustandes. *Arch. Agron. Soil Sci.* **1970**, *14*, 3-14.
13. Tikhonov, V.V.; Orlov, D.S.; Lisovitskaia, O.V.; Zavgorodniaia, I.A.; Byzov, B.A.; Demin, V.V. Sorption of humic acids by bacteria. *Mikrobiologiia* **2013**, *82*, 691-7.
14. Esfahani, M.R.; Stretz, H.A.; Wells, M.J. Abiotic reversible self-assembly of fulvic and humic acid aggregates in low electrolytic conductivity solutions by dynamic light scattering and zeta potential investigation. *Sci Total Environ* **2015**, *15*, 81-92.
15. Filella, M.; Buffle J.; Parthasarathy, N. Humic and fulvic compounds, 2nd ed.; Worsfold, P.; Townshend, A.; Poole, C.; Encyclopedia of Analytical Science, Elsevier, 2005; pp. 288-298.
16. Sanchez, J.C.; DiPasquale, A.G.; Mrse, A.A.; Trogler, W.C. Lewis acid-base interactions enhance explosives sensing in silacycle polymers. *Anal Bioanal Chem* **2009**, *395*, 387-92.
17. Avramenko, V.A.; Bratskaya, S.Y.; Yakushevich, A.S. Humic acids in brown coals from the southern Russian Far East: General characteristics and interactions with precious metals. *Geochem. Int* **2012**, *50*, 437–446.
18. Bratskaya, S.Y.; Volk, A.S.; Ivanov, V.V.; Ustinov, A.Y.; Barinov, N.N.; Avramenko, V.A. A new approach to precious metals recovery from brown coals: Correlation of recovery efficacy with the mechanism of metal–humic interactions. *Geochim cosmochim ac* **2009**,*73*, 3301-3310.
19. Zhernov, Y.V.; Konstantinov, A.I.; Zherebker, A. Antiviral activity of natural humic substances and shilajit materials against HIV-1: Relation to structure. *Environ Res* **2021**,*193*, 110312.
20. Lu, F.J.; Tseng, S.N.; Li, M.L.; Shih, S.R. In vitro anti-influenza virus activity of synthetic humate analogues derived from protocatechuic acid. *Arch. Virol* **2002**, *147*, 273–284.
21. Klocking, R.; Helbig, B.; Schotz, G.; Schacke, M.; Wutzler, P. Anti-HSV-1 activity of synthetic humic acid-like polymers derived from p-diphenolic starting com-pounds. *Antivir. Chem. Chemother* **2002**, *13*, 241–249.
22. Orlov, A.A.; Zherebker, A.; Eletskaya, A.A.; Chernikov, V.S.; Kozlovskaya, L.I.; Zhernov, Y.V.; Kostyukevich Y.; Palyulin, V.A.; Nikolaev, E.N.; Osolodkin, D.I.; Perminova, I.V. Examination of molecular space and feasible structures of bioactive components of humic substances by FTICR MS data mining in ChEMBL database. *Sci. Rep* **2019**,*9*,12066.
23. Rensburg, C. E. J.; Dekker, A. S. J.; An in vitro investigation of the antimicrobial activity of oxifulvic acid. *J Antimicrob Chemother* **2000**, *46*, 853–854.
24. Wu, M.; Song, M.; Liu, M.; Jiang, C.; Li, Z. Fungicidal activities of soil humic/fulvic acids as related to their chemical structures in greenhouse vegetable fields with cultivation chronosequence. *Sci Rep* **2016**, *6*, 32858.
25. Zhernov, Y.V.; Kremb, S.; Helfer, M.; Schindler, M.; Harir, M.; Mueller, C.; Hertkorn, N.; Avvakumova, N.P.; Konstantinov, A.I.; Brack-Werner, R.; Sch mitt-Kopplin, P.; Perminova, I.V. Supramolecular combinations of humic polyanions as potent microbicides with polymodal anti-HIV-activities. *New J. Chem* **2017**, *41*, 212–224.
26. Hafez, M.; Popov, A. I.; Zelenkov, V.N.; Teplyakova, T.V.; Rashad, M. Humic substances as an environmental- friendly organic wastes potentially help as natural anti-virus to inhibit COVID-19. *Science Archives* **2020**, *1*, 53-60.
27. Ph. Eur. 10.0: EDQM, 2019; Volume 2.2.32, pp. 57–58.
28. Hunger, K.; Review of Progress in Coloration and Related Topics. The effect of crystal structure on colour application properties of organic pigments **2008**, *29*, 71-84.
29. Mondal, H.; Mondal, S.; Saha, K.; Roul, B.; Development of a Low-cost Smartphone-connected Digital Microscope. *J Microsc Ultrastruct* **2019**, *29*, 51-54.
30. Zanin, L.; Tomasi, N.; Cesco, S.; Varanini, Z.; Pinton, R.; Humic Substances Contribute to Plant Iron utrition Acting as Chelators and Biostimulants. *Front Plant Sci* **2019**,*10*, 675.
31. Fuentes, M.; Olaetxea, M.; Baigorri, R.; Zamarreno, A. M.; Etienne, P.; Laine, P. Main binding sites involved in Fe(III) and Cu(II) complexation in humic-based structures. *J. Geochem. Exp* **2013**,*129*, 14–17.
32. Gerke, J. Solubilization of Fe(III) from humic-Fe complexes, humic/Fe-oxide mixtures and from poorly ordered Fe-oxide by organic acids - consequences for P adsorption. *Z. Pflanzenernahr. Bodenk* **1993**, *156*, 253–257.
33. Lucena, J. J. Fe chelates for remediation of Fe chlorosis in strategy I plants. *J. Plant Nutr* **2003**, *26*, 1969–1984.
34. Tomasi, N .; Mimmo, T .; Terzano, R .; Alfeld, M .; Janssens, K .; Zanin L. Accumulation of nutrients in leaves of Fe-deficient cucumber plants treated with natural Fe-complexes. Biol Fert Soils **2014**, *50*, 973-982.

35. Kumar, S.; Koh, J. Physiochemical, Optical and Biological Activity of Chitosan-Chromone Derivative for Biomedical Applications. *Int. J. Mol. Sci* **2012**, *13*, 6102-6116.
36. Lim, S.F.; Zheng, Y.M.; Zou, S.W.; Chen, J.P. Characterization of copper adsorption onto an alginate encapsulated magnetic sorbent by a combined FT-IR, XPS, and mathematical modeling study. *Environ. Sci. Technol* **2008**, *42*, 2551–2556.
37. Zeng, S.; Cao, Y.; Sang, W.; Li, T.; Gan, N.; Zheng, L. Enrichment of Polychlorinated Biphenyls from Aqueous Solutions Using Fe3O4 Grafted Multiwalled Carbon Nanotubes with Poly Dimethyl Diallyl Ammonium Chloride. *Int. J. Mol. Sci* **2012**, *13*, 6382-6398.
38. Shi H, N.J.; Sakatsume, T.; Bandow, K.; Okudaira, N.; Uesawa, Y.; Sakagami, H.; Tomomura, M.; Tomomura, A.; Takao, K.; Sugita, Y. Quantitative Structure-Cytotoxicity Relationship of 3-(N-Cyclicamino)chromone *Derivatives. Anticancer Res* **2018**, *38*, 4459-4467.
39. Lewandowski, W.; Lewandowska, H.; Golonko, A.; Swiderski, G.; Swislocka, R.; Kalinowska, M. Correlations between molecular structure and biological activity in "logical series" of dietary chromone derivatives. *PLoS One* **2020**, *15*, 0229477.
40. Tang, Y.; Huang, Y.; Chen, Y.; Lu, L.; Wang, C.; Sun, T.; Wang, M.; Zhu, G.; Yang, Y.; Zhang, L. A coumarin derivative as a "turn-on" fluorescence probe toward Cd2+ in live cells. Spectrochim. *Acta A Mol. Biomol. Spectrosc* **2019**, *218*, 359–365.
41. Wani, M.A.; Singh, P.K.; Pandey, R.; Pandey, M.D. Coumarin-pyrene conjugate: Synthesis, structure and Cu-selective fluorescent sensing in mammalian kidney cells. *J. Lumin* **2016**, *171*, 159–165.
42. Yanar, U.; Babur, B.; Pekyilmaz, D.; Yahaya, I.; Aydiner, B.; Dede, Y.; Seferoglu, Z. A fluorescent coumarin-thiophene hybrid as a ratiometric chemosensor for anions: Synthesis, photophysics, anion sensing and orbital interactions. *J. Mol. Struct* **2016**, *1108*, 269–277.
43. Huang, J.; Yan, Z.; Qiu, P.; Mo, Y.; Cao, Q.; Li, Q.; Huo, L.; Zhao, L. A New Coumarin-Acridone Compound as a Fluorescence Probe for Fe3+ and Its Application in Living Cells and Zebrafish. *Molecules* **2021**, *26*, 2115.
44. Gast, K.; Fiedler, C. Dynamic and Static Light Scattering of Intrinsically Disordered Proteins, 2nd ed.; Uversky, V., Dunker, A., Eds.; Intrinsically Disordered Protein Analysis. Methods in Molecular Biology, Publisher: Springer, New York, **2012**; Volume 896.
45. Tamborini, E.; Cipelletti, L. Multiangle static and dynamic light scattering in the intermediate scattering angle range Citation. *Rev Sci Instrum* **2012**, *83*, 093106.
46. Phanse, Y.; Ramer-Tait, A.E.; Friend, S.L.; Carrillo-Conde, B.; Lueth, P.; Oster, C. J., Phillips, G.J.; Narasimhan, B.; Wannemuehler, M. J.; Bellaire, B. H. Analyzing Cellular Internalization of Nanoparticles and Bacteria by Multi-spectral Imaging Flow Cytometry. *J. Vis. Exp* **2012**, *64*, 3884.
47. Graczyk, A.; Pawlowska, R.; Jedrzejczyk, D.; Chworos, A. Gold Nanoparticles in Conjunction with Nucleic Acids as a Modern Molecular System for Cellular Delivery. *Molecules* **2020**, *25*, 204.
48. Bayda, S.; Adeel, M.; Tuccinardi, T.; Cordani, M.; Rizzolio, F. The History of Nanoscience and Nanotechnology: From Chemical–Physical Applications to Nanomedicine. *Molecules* **2020**, *25*, 112.
49. Mukhtar, I.; Wu, S.; Wei, S.; Chen, R.; Cheng, Y.; Chen, L.; Chen, J.; Transcriptome Profiling Revealed Multiple rqu A Genes in the Species of Spirostomum (Protozoa: Ciliophora: Heterotrichea). *Front in Microbiol* 2021, *11*, 3373.
50. Goncharuk, V.V.; Syroeshkin, A.V.; Zlatskiy, I.A.; Uspenskaya, E.V.; Orekhova, A.V.; Levitskaya, O. V.; Dobrovolskiy, V. I.; Pleteneva, T.V. Quasichemical description of the cell death kinetics of cellular biosensor Spirostomum ambigua for testing the biological activity of aqueous solutions. *J Water Chem Tech* **2017**, *39*, 97–102.
51. Palumbo, G.; Schiavon, M.; Nardi, S.; Ertani, A.; Celano G.; Colombo, C.M. Biostimulant Potential of Humic Acids Extracted From an Amendment Obtained via Combination of Olive Mill Wastewaters (OMW) and a Pre-treated Organic Material Derived From Municipal Solid Waste (MSW). *Front Plant Sci* **2018**, *9*, 1028.
52. Zhou, L.; Yuan, L.; Zhao, B.; Li, Y.; Lin, Z. Structural characteristics of humic acids derived from Chinese weathered coal under different oxidizing conditions. *PLoS One* **2019**,*14*, 0217469.
53. Li, Y.; Guo, L.X.; Zhou, Q.Z. Characterization of Humic Substances in the Soils of Ophiocordyceps sinensis Habitats in the Sejila Mountain, Tibet: Implication for the Food Source of Thitarodes Larvae. *Molecules* **2019**, *24*, 246.
54. Klucakova, M.; Veznikova, K. The Role of Concentration and Solvent Character in the Molecular Organization of Humic Acids. *Molecules* **2016**,*21*, 1410.
55. Melnikova, N.; Solovjevaa, O.; Vorobyovaa, O.; Solovyevab, A.; Peretyaginb, P.; Didenkob, N.; Korobkoa V. The Humic Acids of Peat. Physico-Chemical Properties and Biological Activity in Erythrocytes. *Int. J. Pharm Sci. Rev. Res* **2017**, *45*, 278-856.
56. Pant, K.; Singh, B.; Thakur, N. S. A Humic Matter Panacea for Cancer. *IJTPR* **2012**, *4*, 17-25.
57. Cagno, V.; Donalisio, M.; Civra, A.; Cagliero, C.; Rubiolo, P.; Lembo, D. In vitro evaluation of the antiviral properties of Shilajit and investigation of its mechanisms of action. *J Ethnopharmacol* **2015**, *166*, 129-34.
58. Kwon, P.S.; Oh, H.; Kwon, S.J. Sulfated polysaccharides effectively inhibit SARS-CoV-2 in vitro. *Cell Discov* **2020**, 6, 50.
59. Gupta, A.K.; Gupta, M. Synthesis and surface engineering of iron oxide nanoparticles for biomedical applications. *Biomaterials* **2005**, *26*, 3995–4021.
60. Limbach, L.K.; Li, Y.; Grass, R.N.; Brunner, T.J.; Hintermann, M.A.; Muller, M.; Gunther, D.; Stark, W.J. Oxide nanoparticle uptake in human lung fibroblasts: Effects of particle size, agglomeration, and diffusion at low concentrations. Environ. *Sci. Technol* **2005**, *39*, 9370–9376.
61. Giachin, G.; Nepravishta, R.; Mandaliti, W. The mechanisms of humic substances self-assembly with biological molecules: The case study of the prion protein. *PLoS One* **2017**, *12*, 0188308.

62. Yoon, H.Y.; Lee, J.G.; Esposti, L.D. Synergistic Release of Crop Nutrients and Stimulants from Hydroxyapatite Nanoparticles Functionalized with Humic Substances: Toward a Multifunctional Nanofertilizer. *ACS Omega* **2020**, *5*, 6598-6610.
63. Szabo, O.E.; Csiszar, E.; Toth, K.; Szakacs, G.; Koczka, B. Ultrasound-assisted extraction and characterization of hydrolytic and oxidative enzymes produced by solid state fermentation. *Ultrason Sonochem* **2015,** *22*, 249-56.
64. Reed, L.; Muench, H. A simple method of estimating fifty per cent endpoints. *Am J Emerg* **1938**, 27, 493–97.
65. Xu, K.; Martinez, M.M.; Yang, B.; Guo, M. Fine structure, physicochemical and antioxidant properties of LM-pectins from okra pods dried under different techniques. *Carbohydr Polym* **2020**, *241*, 116272.
66. Odnovorov, A. I.; Grebennikova, T. V.; Pleteneva, T. V.; Garaev, T. M.; Uspenskaya, E. V.; Khodorovich, N. A.; Levitskaya, O. V.; Koldina, A. M. Physicochemical properties and biological hysicochemical properties and Hysicochemical properties and biological activity of the new antiviral substance. *Int J App Pharm* **2020**, *12*, 237-242.
67. Ismatullaev, A.; Taşın, S.; Usumez, A. Evaluation of bond strength of resin cement to Er:YAG laser-etched enamel and dentin after cementation of ceramic discs. *Lasers Med Sci* **2021**, *36*, 447-454.
68. Morozova, M. A.; Koldina, A. M.; Maksimova, T. V.; Marukhlenko, A. V.; Zlatsky, I. A.; Syroeshkin, A. V. Slow quasikinetic changes in water-lactose complexes during storage. *Int J App Pharm* **2021**, *13*, 227-232.
69. Syroeshkin, A.V.; Uspenskaya, E.V.; Pleteneva, T.V.; Morozova, M.A.; Zlatskiy, I.A.; Koldina, A.M.; Nikiforova, M.V. Mechanical Transformation of Compounds Leading to Physical, Chemical, and Biological Changes in Pharmaceutical Substances. *Sci. World. J* **2018**, *8905471*, 8.
70. Ph. Eur. 10.0: EDQM, 2019; Volume 2.2.32, pp. 39–42.
71. Vo, A.; Feng, X.; Smith, W.C.; Zhu, D.; Patel, M.; Kozak, D.; Wang, Y.; Zheng, J.; Ashraf, M.; Xu, X. Analyzing ophthalmic suspension particle size distributions using laser diffraction: Placebo background subtraction method. *Int J Pharm* **2021**, *1*, 120401.
72. Ishmatov, A.N.; Akhmadeev, I.R. The low-angle laser light scattering method in the study of pulse liquid atomization. *Atmos Ocean Opt* **2013**, *26*, 444–448.
73. Uspenskaya, E.V.; Pleteneva, T.V.; Kazimova, I.V.; Syroeshkin, A.V. Evaluation of Poorly Soluble Drugs' Dissolution Rate by Laser Scattering in Different Water Isotopologues. *Molecules* **2021**, *26*, 601.
74. Zhdanov, V.P. How the partial-slip boundary condition can influence the interpretation of the DLS and NTA data. *J Biol Phys* **2020**, *46*, 169-176.
75. Zlatskiy, I.; Pleteneva, T.; Skripnikov, A.; Grebennikova, T.; Maksimova, T.; Antipova, N.; Levitskaya, O.; Makarova, M.; Selivanenko, I.; Syroeshkin, A. Dependence of Biocatalysis on D/H Ratio: Possible Fundamental Differences for High-Level Biological Taxons. *Molecules* **2020**, 11;25(18):4173.
76. Mukhtar, I.; Wu, S.; Wei, S.; Chen, R.; Cheng, Y.; Liang, C.; Chen, J. Transcriptome Profiling Revealed Multiple rquA Genes in the Species of Spirostomum (Protozoa: Ciliophora: Heterotrichea). *Front Microbiol* **2021**, *5*, 574285.
77. Uspenskaya, E.V.; Pleteneva, T.V.; Syroeshkin, A.V.; Taravrina, I.V.; Preparation, characterization and studies of physicochemical and biological properties of drugs coating lactose in fluidized beds. *Int J App Pharm* **2020**, *12*, 272-278.